

Cho-Maison Monopole-antimonopole Pair in Standard Model

Dan Zhu, Khai-Ming Wong and Guo-Quan Wong

School of Physics, Universiti Sains Malaysia, 11800 USM, Penang, Malaysia

We present numerical solutions corresponding to a pair of Cho-Maison monopole and antimonopole (MAP) in the $SU(2) \times U(1)$ Weinberg-Salam (WS) theory, which possess magnetic charge $\pm 4\pi/e$. The system was investigated at physical Weinberg angle, $\tan \theta_w = 0.53557042$, while the Higgs self-coupling constant, $0 \leq \beta \leq 1.7704$ and at physical $\beta = 0.77818833$, while $0.4675 \leq \tan \theta_w \leq 10$. Numerical data was compared with MAP solutions found in the $SU(2)$ Yang-Mills-Higgs (YMH) theory. Magnetic dipole moment (μ_m), pole separation (d_z) and Higgs modulus at the origin (z_0) of the numerical solutions are calculated and analyzed. A major difference exists between these two types of MAP, where for Cho-Maison MAP, there exists an upper bound ($\beta = 1.7704$) after which no solution can be found, a feature not present in the $SU(2)$ MAP configuration.

Magnetic monopoles remained a topic of extensive studies ever since P.A.M. Dirac [1] introduced the idea into Maxwell's theory. It was generalized to non-Abelian gauge theories in 1968 by Wu and Yang [2]. However, both Dirac and Wu-Yang monopoles possess infinite energy due to the presence of a point singularity at the origin. The first finite energy magnetic monopole solution is the 't Hooft-Polyakov monopole [3] in the $SU(2)$ YMH theory, found independently by G. 't Hooft and A.M. Polyakov in 1974. The mass of their monopole was estimated to be around $137 m_w$, where m_w is the mass of intermediate vector boson.

Since then, numerous solutions were found in the $SU(2)$ YMH theory. In the BPS limit with vanishing Higgs potential, there exist exact monopole [4] and multimonopole [5] solutions. Other well-known cases are the axially symmetric MAP of Kleihaus and Kunz [6], and the monopole-antimonopole chain (MAC) of Kleihaus et al. [7]. These solutions possess finite energy and represent a chain of magnetic monopoles and antimonopoles lying in alternating order along the symmetrical axis.

Magnetic monopole research started a new chapter when the electroweak Cho-Maison monopole [8] was reported. The mass of Cho-Maison monopole is infinite due to the point singularity at the origin. However, it has been shown that the solution can be regularized and the mass was estimated to be around 4 to 10 TeV [9]. More recently, different methods were used to regularize the solution, it is reported that the new BPS bound for Cho-Maison monopole may not be smaller than 2.98 TeV, more probably 3.75 TeV [10]. Another estimate puts the lower bound of the mass of Cho-Maison monopole at 2.37 TeV [11].

The importance of the Cho-Maison monopole follows from the following facts. First, as the electroweak generalization of the Dirac monopole, it must exist if the Standard Model is correct [8, 9]. Moreover, the prediction of the mass strongly indicates that it could actually be produced at LHC in the near future. So, when discovered, it will become the first magnetically charged topological elementary particle in the history of physics. Second, it

could have deep implications in cosmology. This is because it could induce the density perturbation in the early universe and generate primordial magnetic black holes which could explain the dark matter. As importantly, it could become the seed of the large scale structures of the universe and become the source of the intergalactic magnetic field [12]. For these reasons MoEDAL and ATLAS at LHC are actively searching for the monopole [13, 14].

In 1977, Y. Nambu theoretically demonstrated the existence of a pair of magnetic monopole and antimonopole bound by a flux string in the $SU(2) \times U(1)$ WS theory [15]. Numerical solutions of Nambu MAP [16, 17] were constructed using the axially symmetric magnetic ansatz of Ref. [6] coupled with an appropriate $U(1)$ gauge field.

The magnetic charge carried by each pole of the Nambu MAP is a fraction, $\pm \frac{4\pi}{e} \sin^2 \theta_w$. In contrast, the poles of Cho-Maison MAP in this paper carry non-fractional magnetic charge of $\pm \frac{4\pi}{e}$. The MAP configuration was investigated at physical Weinberg angle, $\tan \theta_w = 0.53557042$, while the Higgs self-coupling constant, β , runs from 0 to 1.7704 and at physical $\beta = 0.77818833$, while $\tan \theta_w$ is allowed to vary ($0.4675 \leq \tan \theta_w \leq 10$). For better comparison, numerical solutions found in the $SU(2) \times U(1)$ WS theory were compared with MAP solutions of Kleihaus and Kunz [6] when ϕ -winding number, $n = 1$. The investigated quantities include magnetic dipole moment (μ_m), pole separation (d_z) and the Higgs modulus at the origin (z_0).

The Lagrangian of $SU(2) \times U(1)$ WS theory is given by [8][16]

$$\mathcal{L} = -\frac{1}{4} F_{\mu\nu}^a F^{a\mu\nu} - \frac{1}{4} G_{\mu\nu} G^{\mu\nu} - (\mathcal{D}_\mu \phi)^\dagger (\mathcal{D}^\mu \phi) - \frac{\lambda}{2} \left(\phi^\dagger \phi - \frac{\mu_H^2}{\lambda} \right)^2. \quad (1)$$

Here, \mathcal{D}_μ is the covariant derivative of $SU(2) \times U(1)$ group and is defined as

$$\mathcal{D}_\mu = D_\mu - \frac{i}{2} g' B_\mu = \partial_\mu - \frac{i}{2} g A_\mu^a \sigma_a - \frac{i}{2} g' B_\mu, \quad (2)$$

where D_μ is the covariant derivative of SU(2) group only.

The SU(2) gauge coupling constant, potential and electromagnetic tensor are g , A_μ^a and $F_{\mu\nu}^a$. Their counterparts in U(1) gauge field are denoted as g' , B_μ and $G_{\mu\nu}$. The term, σ_a , is the Pauli matrices, ϕ and λ are the complex scalar Higgs doublet and Higgs field self-coupling constant. Higgs boson mass and μ_H are related through $m_H = \sqrt{2}\mu_H$. In addition, the Higgs field can be expressed as $\phi = H\xi/\sqrt{2}$, where ξ is a column 2-vector that satisfies $\xi^\dagger \xi = 1$. Metric used in this paper is $(-+++)$.

Through Lagrangian (1), three equations of motion can be obtained as the following,

$$\mathcal{D}^\mu \mathcal{D}_\mu \phi = \lambda \left(\phi^\dagger \phi - \frac{\mu_H^2}{\lambda} \right) \phi, \quad (3)$$

$$D^\mu F_{\mu\nu}^a = \frac{ig}{2} \left[\phi^\dagger \sigma^a (\mathcal{D}_\nu \phi) - (\mathcal{D}_\nu \phi)^\dagger \sigma^a \phi \right], \quad (4)$$

$$\partial^\mu G_{\mu\nu} = \frac{ig'}{2} \left[\phi^\dagger (\mathcal{D}_\nu \phi) - (\mathcal{D}_\nu \phi)^\dagger \phi \right]. \quad (5)$$

The magnetic ansatz used to obtain the Cho-Maison MAP is:

$$\begin{aligned} gA_i^a &= -\frac{1}{r} \psi_1(r, \theta) \hat{n}_\phi^a \hat{\theta}_i + \frac{n}{r} \psi_2(r, \theta) \hat{n}_\theta^a \hat{\phi}_i \\ &\quad + \frac{1}{r} R_1(r, \theta) \hat{n}_\phi^a \hat{r}_i - \frac{n}{r} R_2(r, \theta) \hat{n}_r^a \hat{\phi}_i, \\ g'B_i &= \frac{n}{r \sin \theta} B_s(r, \theta) \hat{\phi}_i, \quad gA_0^a = g'B_0 = 0, \\ \Phi^a &= \Phi_1(r, \theta) \hat{n}_r^a + \Phi_2(r, \theta) \hat{n}_\theta^a = H(r, \theta) \hat{\Phi}^a. \end{aligned} \quad (6)$$

Additionally, the Higgs unit vector, $\hat{\Phi}^a$, can be expressed as,

$$\begin{aligned} \hat{\Phi}^a &= -\xi^\dagger \sigma^a \xi \\ &= \cos(\alpha - \theta) \hat{n}_r^a + \sin(\alpha - \theta) \hat{n}_\theta^a = h_1 \hat{n}_r^a + h_2 \hat{n}_\theta^a, \\ \xi &= i \begin{pmatrix} \sin \frac{\alpha(r, \theta)}{2} e^{-in\phi} \\ -\cos \frac{\alpha(r, \theta)}{2} \end{pmatrix}. \end{aligned} \quad (7)$$

The functions, $\cos \alpha$ and $\sin \alpha$ are defined as

$$\begin{aligned} \cos \alpha &= \frac{\Phi_1 \cos \theta - \Phi_2 \sin \theta}{\sqrt{\Phi_1^2 + \Phi_2^2}} = h_1 \cos \theta - h_2 \sin \theta, \\ \sin \alpha &= \frac{\Phi_1 \sin \theta + \Phi_2 \cos \theta}{\sqrt{\Phi_1^2 + \Phi_2^2}} = h_1 \sin \theta + h_2 \cos \theta. \end{aligned} \quad (8)$$

Moreover, the angle, $\alpha(r, \theta) \rightarrow p\theta$ asymptotically [16], where p is the parameter controlling the number of poles in the solution and is set to two. Finally, $H(r, \theta) = |\Phi| = \sqrt{\Phi_1^2 + \Phi_2^2}$ is the Higgs modulus.

In the magnetic ansatz, the spatial spherical coordinate unit vectors are defined as

$$\begin{aligned} \hat{r}_i &= \sin \theta \cos \phi \delta_{i1} + \sin \theta \sin \phi \delta_{i2} + \cos \theta \delta_{i3}, \\ \hat{\theta}_i &= \cos \theta \cos \phi \delta_{i1} + \cos \theta \sin \phi \delta_{i2} - \sin \theta \delta_{i3}, \\ \hat{\phi}_i &= -\sin \phi \delta_{i1} + \cos \phi \delta_{i2}. \end{aligned} \quad (9)$$

Similarly, the unit vectors for isospin coordinate system are given by

$$\begin{aligned} \hat{n}_r^a &= \sin \theta \cos n\phi \delta_1^a + \sin \theta \sin n\phi \delta_2^a + \cos \theta \delta_3^a, \\ \hat{n}_\theta^a &= \cos \theta \cos n\phi \delta_1^a + \cos \theta \sin n\phi \delta_2^a - \sin \theta \delta_3^a, \\ \hat{n}_\phi^a &= -\sin n\phi \delta_1^a + \cos n\phi \delta_2^a, \end{aligned} \quad (10)$$

where n is the ϕ -winding number and is set to one in this research.

Upon substituting the magnetic ansatz (6) into the equations of motion (3) - (5), the system of equations was reduced to seven coupled second-order partial differential equations, which were further simplified with the following substitutions,

$$x = m_w r, \quad \tilde{H} = \frac{H}{H_0}, \quad \tan \theta_w = \frac{g'}{g}, \quad \beta^2 = \frac{\lambda}{g^2}. \quad (11)$$

Here $H_0 = \sqrt{2}\mu_H/\sqrt{\lambda}$ and $m_w = gH_0/2$. The new radial coordinate, x , is dimensionless, which is then compactified through $\tilde{x} = x/(x+1)$. The rescaled Higgs field, \tilde{H} , approaches one asymptotically. Only two free parameters were left after the transformation, $\tan \theta_w$ and β . Both of these parameters can be expressed in terms of the mass of elementary particles and by adopting $m_H = 125.10$ GeV, $m_w = 80.379$ GeV and $m_z = 91.1876$ GeV [18], these parameters are calculated to be $\beta = 0.77818833$ and $\tan \theta_w = 0.53557042$.

The seven coupled equations are then subject to the following boundary conditions. Along the positive and negative z -axis, when $\theta = 0$ and π ,

$$\partial_\theta \psi_A = R_A = \partial_\theta \Phi_1 = \Phi_2 = \partial_\theta B_s = 0, \quad (12)$$

where $A = 1, 2$. Asymptotically, when r approaches infinity,

$$\begin{aligned} \psi_A(\infty, \theta) &= 2, \quad R_A(\infty, \theta) = B_s(\infty, \theta) = 0, \\ \Phi_1(\infty, \theta) &= \cos \theta, \quad \Phi_2(\infty, \theta) = \sin \theta, \end{aligned} \quad (13)$$

and finally, at the origin,

$$\begin{aligned} \psi_A(0, \theta) &= R_A(0, \theta) = 0, \quad B_s(0, \theta) = -2, \\ \Phi_1(0, \theta) \sin \theta + \Phi_2(0, \theta) \cos \theta &= 0, \\ \partial_r (\Phi_1(r, \theta) \cos \theta - \Phi_2(r, \theta) \sin \theta) |_{r=0} &= 0. \end{aligned} \quad (14)$$

Note here, due to $B_s(0, \theta) = -2$, the part of magnetic ansatz (6) for $g'B_i$ has a point singularity at the origin, which renders the total energy of the system divergent and therefore cannot be evaluated.

Using finite difference approximation method, the set of seven coupled partial differential equations was converted into a system of non-linear equations, which was then discretized onto a non-equidistant grid of $M \times N$, where $M = 70$, $N = 60$. The region of integration covers all space which translates to $0 \leq \tilde{x} \leq 1$ and $0 \leq \theta \leq \pi$.

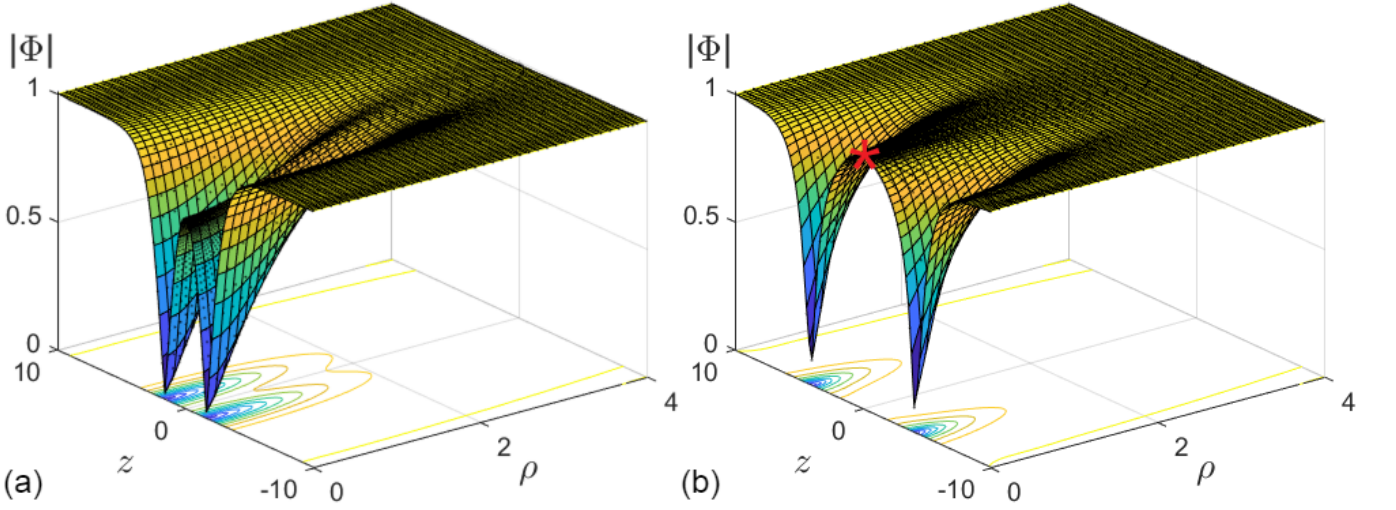


FIG. 1. 3D Higgs modulus plots of (a) an MAP found in the SU(2) YMH theory and (b) a Cho-Maison MAP found in the SU(2)×U(1) WS theory, both with $\beta = 0.77818833$. For the Cho-Maison MAP, $\tan \theta_w = 0.53557042$.

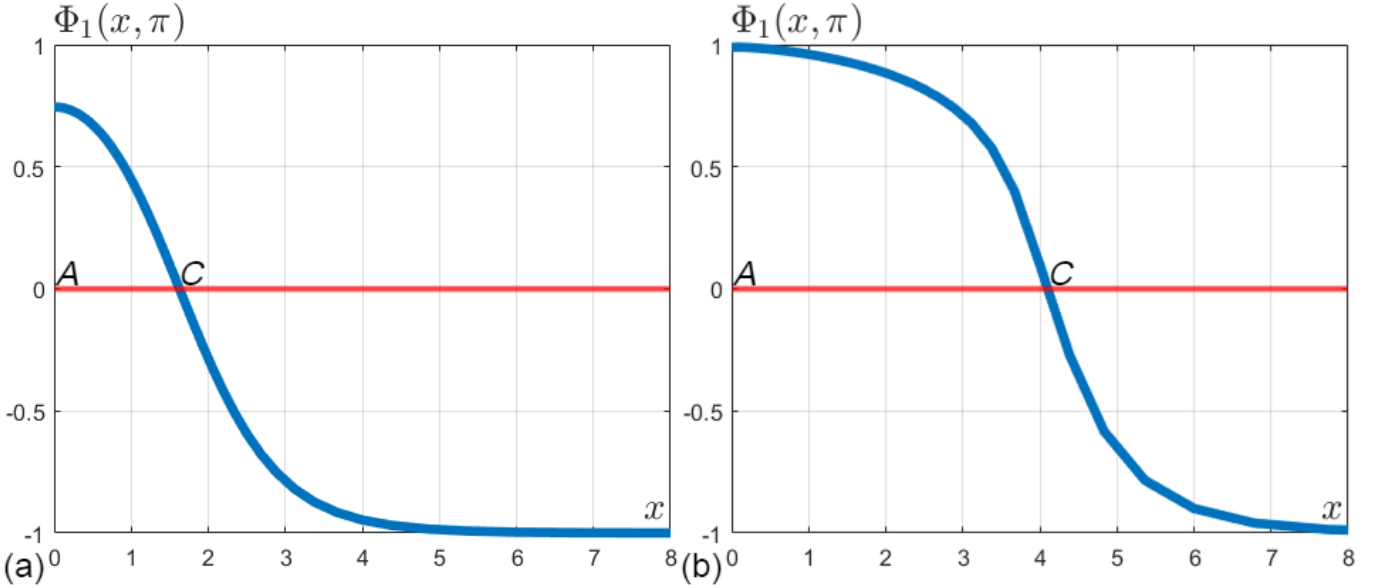


FIG. 2. Curves of $\Phi_1(x, \pi)$ versus x for (a) the SU(2) MAP and (b) the Cho-Maison MAP shown in Fig. 1.

Good initial guesses are needed in order for the numerical computation to converge.

By applying the gauge below, the gauge potential and Higgs field are transformed:

$$\begin{aligned}
 G &= -i \begin{pmatrix} \cos \frac{\alpha}{2} & \sin \frac{\alpha}{2} e^{-in\phi} \\ \sin \frac{\alpha}{2} e^{in\phi} & -\cos \frac{\alpha}{2} \end{pmatrix} \\
 &= \cos \frac{-\pi}{2} + i \hat{u}_r^a \sigma^a \sin \frac{-\pi}{2}, \\
 \hat{u}_r^a &= \sin \frac{\alpha}{2} \cos n\phi \delta_1^a + \sin \frac{\alpha}{2} \sin n\phi \delta_2^a + \cos \frac{\alpha}{2} \delta_3^a. \quad (15)
 \end{aligned}$$

The transformed gauge potential has the following form:

$$\begin{aligned}
 gA_i^a &= -\frac{2n}{r} \left[\psi_2 \sin \left(\theta - \frac{\alpha}{2} \right) + R_2 \cos \left(\theta - \frac{\alpha}{2} \right) \right] \hat{u}_r^a \hat{\phi}_i \\
 &\quad - gA_i^a + \frac{2n \sin \frac{\alpha}{2}}{r \sin \theta} \hat{u}_\theta^a \hat{\phi}_i - \partial_i \alpha \hat{u}_\phi^a. \quad (16)
 \end{aligned}$$

Note here, when $a = 3$, equation (16) becomes the 't Hooft gauge potential,

$$\begin{aligned}
 gA_i^3 &= \frac{n}{r} \left(\psi_2 h_2 - R_2 h_1 - \frac{1 - \cos \alpha}{\sin \theta} \right) \hat{\phi}_i \\
 &= \frac{A_s}{r \sin \theta} \hat{\phi}_i. \quad (17)
 \end{aligned}$$

Now, as

$$\begin{aligned} \begin{pmatrix} A_i^{\text{em}} \\ Z_i \end{pmatrix} &= \begin{pmatrix} \cos \theta_w & \sin \theta_w \\ -\sin \theta_w & \cos \theta_w \end{pmatrix} \begin{pmatrix} B_i \\ A_i'^3 \end{pmatrix} \\ &= \frac{1}{\sqrt{g'^2 + g^2}} \begin{pmatrix} g & g' \\ -g' & g \end{pmatrix} \begin{pmatrix} B_i \\ A_i'^3 \end{pmatrix}, \end{aligned} \quad (18)$$

the real electromagnetic potential could be expressed as

$$eA_i^{\text{em}} = \cos^2 \theta_w (g' B_i) + \sin^2 \theta_w (g A_i'^3), \quad (19)$$

where e is the unit electric charge. The ‘em’ magnetic field could then be calculated according to the mixing shown in equation (19),

$$\begin{aligned} B_i^{\text{em}} &= -\frac{1}{2} \varepsilon_{ijk} F_{jk}^{\text{em}} \\ &= -\frac{1}{e} \varepsilon_{ijk} \partial_j \{ \cos^2 \theta_w B_s + \sin^2 \theta_w A_s \} \partial_k \phi, \end{aligned} \quad (20)$$

and through Gauss’s law, the magnetic charge enclosed in a Gaussian surface, S , with surface element, dS^i , can be obtained with the following integral:

$$Q_{M(S)} = \oint_S B_i^{\text{em}} dS^i = \iiint_V \partial^i B_i^{\text{em}} dV, \quad (21)$$

and for the magnetic charge enclosed in the upper hemisphere, the following Gaussian surface was defined:

$$S_+ = H_+^2 \cup D_{xy}^2, \quad (22)$$

where H_+^2 is a half sphere above the xy -plane and D_{xy}^2 denotes a disk in the xy -plane centered at the origin, both H_+^2 and D_{xy}^2 have the same radius. Taking into account the correct orientation of the surface elements, the magnetic charge enclosed can be calculated as:

$$\begin{aligned} Q_{M(S_+)} &= \iint_{H_+^2} B_i^{\text{em}} r^2 \sin \theta d\theta d\phi \hat{r}^i \\ &\quad - \iint_{D_{xy}^2} B_i^{\text{em}} r dr d\phi \hat{z}^i. \end{aligned} \quad (23)$$

Upon applying the boundary conditions (12) - (14), the first integral vanishes, while the second one becomes:

$$\begin{aligned} \iint_{D_{xy}^2} B_i^{\text{em}} r dr d\phi \hat{z}^i &= \frac{2\pi}{e} \left[\cos^2 \theta_w (-2) + \sin^2 \theta_w (-2) \right] \\ &= -\frac{4\pi}{e}. \end{aligned} \quad (24)$$

Therefore, the magnetic charge carried by the monopole in the upper space is $Q_{M(S_+)} = 4\pi/e$, which is characteristic of a Cho-Maison monopole. Similar calculation shows that magnetic charge in the lower space is $Q_{M(S_-)} = -4\pi/e$.

Additionally, the magnetic dipole moment, μ_m , of a Cho-Maison MAP can be calculated according to the

mixing shown in equation (19) and considering at large r , $g' B_i = g A_i'^3$,

$$A_i^{\text{em}} \longrightarrow \frac{1}{e} (g' B_i) = \frac{1}{e} \frac{n B_s}{r \sin \theta} \hat{\phi}_i. \quad (25)$$

Here, we perform an asymptotic expansion,

$$n B_s \longrightarrow -\frac{\mu_m \sin^2 \theta}{r}, \quad (26)$$

and therefore, $\mu_m = -nr B_s / \sin^2 \theta$. The value of μ_m (in unit of $1/(e \cdot m_w)$) is evaluated at $\theta = \pi/2$.

Figure 1 shows a direct comparison of the Higgs modulus for two MAP solutions found in (a) SU(2) YMH theory and (b) SU(2) × U(1) WS theory, in which ρ -axis is defined as $\rho = \sqrt{x^2 + y^2}$. Physical Higgs self-coupling constant $\beta = 0.77818833$ was chosen for both MAP configurations and physical Weinberg angle $\tan \theta_w = 0.53557042$ was used for the one shown in Fig. 1(b). Visually, the pole separation, d_z , of a Cho-Maison MAP is significantly larger than that of an MAP found in the SU(2) YMH theory. Additionally, the Higgs modulus at the origin (marked with an asterisk in Fig. 1(b) and denoted as z_0) for all solutions found is also measured and plotted.

Numerically, d_z can be measured from the curve of $\Phi_1(x, 0)$ or $\Phi_1(x, \pi)$. This is because $\Phi_2(x, \theta)$ is zero along the z -axis as defined in boundary condition (12) and thus, the behavior of $|\Phi|$ when $\theta = 0$ or π can be shown using profile function Φ_1 alone. Figure 2 shows the curves of $\Phi_1(x, \pi)$ for the two MAPs shown in Fig. 1. In both cases, one of the monopoles is located at $\Phi_1(x, \pi) = 0$, which is labelled as point C in Fig. 2. The pole separation can be defined as $d_z = 2 \times AC$.

By fixing Weinberg angle at $\tan \theta_w = 0.53557042$, the Cho-Maison MAP configuration is investigated for a range of β from 0 to 1.7704. It is found that d_z varies with β and the plot is shown in Fig. 4(a). The value of d_z starts off as 9.7140 when $\beta = 0$, then monotonically decreases until $\beta_{\min} = 1.25$, where the local minimum $d_z = 8.0920$ (green dot) is reached. The physical $\beta = 0.77818833$ is within the range of $0 \leq \beta \leq 1.25$ and d_z is measured to be 8.2012 (red dot). Instead of reaching a constant value, d_z increases again after $\beta_{\min} = 1.25$ until $\beta_c = 1.7704$, where no solution can be found for $\beta > \beta_c$. The corresponding value for d_z when $\beta = \beta_c$ is 8.2760. The behavior of d_z near β_c is shown in Fig. 4(b). For comparison, the plot of d_z versus β for an SU(2) MAP is shown in Fig. 4(c), in which a local minimum is observed around $\beta = 0.6$. This, however, does not occur in the case of Cho-Maison MAP. Additionally, β does not have a critical value, β_c , for an SU(2) MAP.

The plot of μ_m versus β for a Cho-Maison MAP is shown in Fig. 3(a). The shape of the curve is virtually identical to Fig. 4(a), which is expected, considering the close relations between μ_m and d_z . The physical value is measured to be $\mu_m = 8.5514$ (red dot), while

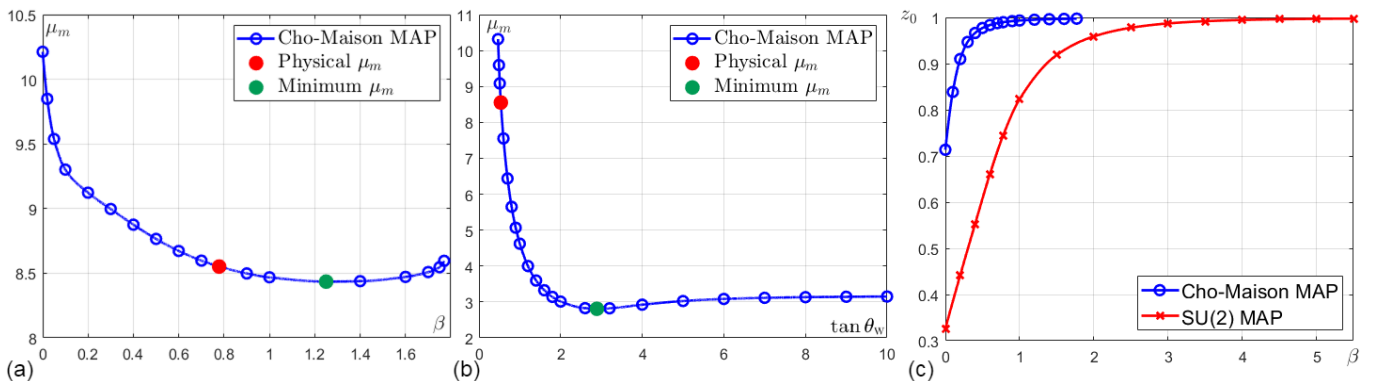


FIG. 3. Plots of (a) μ_m versus β when $\tan\theta_w = 0.53557042$, (b) μ_m versus $\tan\theta_w$ when $\beta = 0.77818833$ for Cho-Maison MAP and (c) the comparison plot of z_0 versus β between Cho-Maison and SU(2) MAPs.

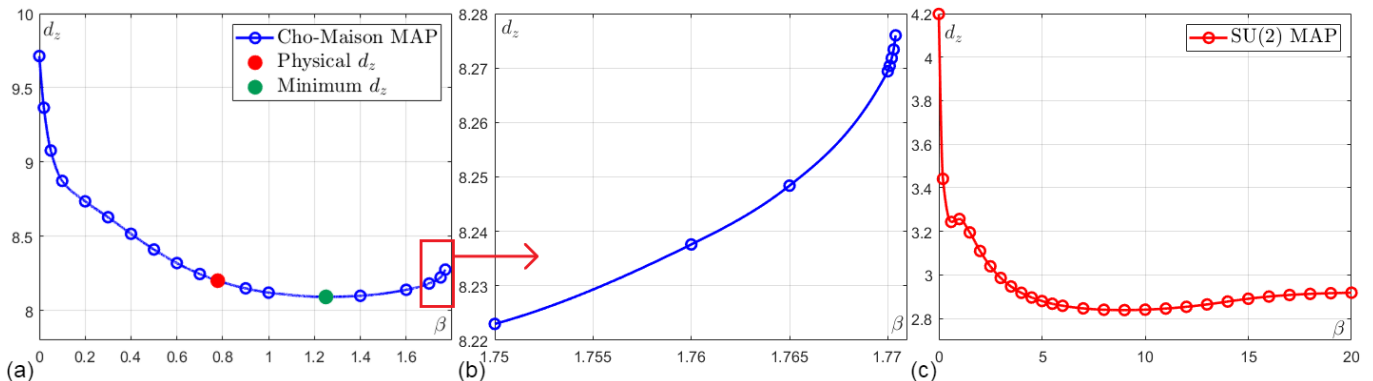


FIG. 4. Plots of d_z versus β for (a) a Cho-Maison MAP, (b) a zoomed-in version of the highlighted region shown in Fig. 4(a) and (c) an SU(2) MAP.

the minimum μ_m is 8.4350 around $\beta_{\min} = 1.25$ (green dot). We also investigate the behavior of μ_m by fixing $\beta = 0.77818833$, while allowing $\tan\theta_w$ to range between 0.4675 and 10, Fig. 3(b). It is found that $\mu_m \rightarrow 10.3178$ as $\tan\theta_w \rightarrow 0.4675$, where a lower bound is reached, below which no solution can be found. In a similar manner, μ_m decreases until $\tan\theta_w = 2.89$, then increases slightly with increasing $\tan\theta_w$ before converging to a limiting value. The minimum value found this way is much lower, $\mu_m = 2.8098$ (green dot). Finally, a comparison of z_0 versus β between the two MAPs is shown in Fig. 3(c). The value of z_0 for a Cho-Maison MAP starts off higher and approaches one significantly faster as compared to an SU(2) MAP. Selected data of Cho-Maison MAP is tabulated in Table I and II.

In conclusion, we have found numerical solutions in the SU(2) \times U(1) WS theory corresponding to a pair of Cho-Maison monopoles, which carry magnetic charge $\pm 4\pi/e$. Unfortunately, due to the presence of a point singularity in the U(1) gauge field, the energy of the system cannot be evaluated. In the case of a single Cho-Maison monopole, it is possible to regularize the singularity by introducing a non-trivial U(1) hypercharge permeability

in the form of a dimensionless function, $\epsilon(\phi) = (H/H_0)^8$ [9, 10], where $H = \sqrt{\Phi_1^2 + \Phi_2^2}$ is the modulus of Higgs field. With $H \rightarrow 0$ as $r \rightarrow 0$, $\epsilon(\phi)$ approaches zero fast enough to eliminate the singularity and rendering the energy density integrable. However, such a choice of $\epsilon(\phi)$ is no longer viable in the MAP configuration reported here as $H/H_0 \rightarrow z_0 \neq 0$.

The major difference between a Cho-Maison MAP and one found in the SU(2) YMH theory is the existence of a critical value, β_c , in a Cho-Maison MAP. When $\tan\theta_w$ is fixed at 0.53557042 and $\beta > \beta_c = 1.7704$, no solution can be found. That is, there appears to be an upper-bound for β after which no solution can be found, which is in stark contrast to an SU(2) MAP. Unlike solutions found in the SU(2) YMH theory, the Cho-Maison MAP is controlled by two parameters, β and $\tan\theta_w$. Therefore, if the lowest possible value of d_z is to be obtained, one must find the global minimum on a 2-dimensional curve of $d_z(\tan\theta_w, \beta)$. Additionally, a lower bound exists at $\tan\theta_w = 0.4675$, where both μ_m and d_z reach their maximum values of 10.3178 and 9.9384. Lastly, we were able to accurately measure the physical value of μ_m and d_z . The magnetic dipole moment of a Cho-Maison MAP is

TABLE I. Table of μ_m , d_z and z_0 for selected β of Cho-Maison MAP solutions at physical Weinberg angle $\tan \theta_w = 0.53557042$.

β	0	0.2	0.4	0.6	0.77818833	0.9	1	1.25	1.4	1.6	1.7704
μ_m	10.2122	9.1227	8.8754	8.6719	8.5514	8.4983	8.4684	8.4350	8.4385	8.4715	8.5958
d_z	9.7140	8.7356	8.5170	8.3198	8.2012	8.1496	8.1208	8.0920	8.0994	8.1398	8.2760
z_0	0.7135	0.9099	0.9663	0.9835	0.9897	0.9920	0.9933	0.9954	0.9961	0.9968	0.9974

TABLE II. Table of μ_m and d_z for selected $\tan \theta_w$ of Cho-Maison MAP solutions at physical Higgs self-coupling constant $\beta = 0.77818833$.

$\tan \theta_w$	0.4675	0.53557042	0.6	0.8	1	2	2.89	4	6	8	10
μ_m	10.3178	8.5514	7.5528	5.6489	4.6219	3.0113	2.8098	2.9240	3.0831	3.1329	3.1513
d_z	9.9384	8.2012	7.2484	5.4582	4.4912	2.8624	2.6120	2.7568	2.9584	3.0228	3.0470

$\mu_m = 8.5514$ in unit of $1/(e \cdot m_w)$ and the pole separation is $d_z = 8.2012$ in unit of $1/m_w$.

As a final note, we will continue working on finding the specific form of $\epsilon(\phi)$ suitable for the Cho-Maison MAP configuration in order to regularize the solution and evaluate the total energy of the system. This will be reported in a future work.

-
- [1] P.A.M. Dirac, Proc. R. Soc. Lond. A **133**, 60 (1931); Phys. Rev. **74**, 817 (1948).
- [2] T.T. Wu and C.N. Yang, in *Properties of Matter under Unusual Conditions*, edited by H. Mark and S. Fernbach (Interscience, New York, 1969), p. 349; Nucl. Phys. B **107**, 365 (1976); Phys. Rev. D **16**, 1018 (1977).
- [3] G. 't Hooft, Nucl. Phys. B **79**, 276 (1974); A.M. Polyakov, JETP Lett. **20**, 194 (1974).
- [4] M.K. Prasad and C.M. Sommerfield, Phys. Rev. Lett. **35**, 760 (1975).
- [5] P. Forgács, Z. Horváth, and L. Palla, Phys. Lett. B **99**, 232 (1981); M. K. Prasad and P. Rossi, Phys. Rev. D **24**, 2182 (1981).
- [6] B. Kleihaus and J. Kunz, Phys. Rev. D **61**, 025003 (1999).
- [7] B. Kleihaus, J. Kunz and Y. Shnir, Phys. Lett. B **570**, 237 (2003); Phys. Rev. D **70**, 065010 (2004).
- [8] Y.M. Cho, D. Maison, Phys. Lett. B **391**, 360 (1997); Yisong Yang, Proc. Roy. Soc. **A454**, 155 (1998); *Solitons in Field Theory and Nonlinear Analysis* (Springer Monographs in Mathematics), p. 322 (Springer-Verlag) 2001.
- [9] Kyoungtae Kimm, J.H. Yoon, and Y.M. Cho, Eur. Phys. J. **C75**, 67 (2015); Kyoungtae Kimm, J. H. Yoon, S. H. Oh and Y. M. Cho, Mod. Phys. Lett. A **31**, 1650053 (2016).
- [10] P. Zhang, L. Zou, Y. M. Cho, Eur. Phys. J. C **80**, 280 (2020).
- [11] F. Blaschke and P. Benes, Prog. Theor. Exp. Phys. 073B03 (2018).
- [12] Y. M. Cho, Phil. Trans. R. Soc. **A377**, 0038 (2019).
- [13] B. Acharya et al. (MoEDAL Collaboration), Phys. Rev. Lett. **118**, 061801 (2017); Phys. Rev. Lett. **123**, 021802 (2019); Phys. Rev. Lett. **126**, 071801 (2021).
- [14] ATLAS Collaboration, Phys. Rev. Lett. **124**, 031802 (2020).
- [15] Y. Nambu, Nucl. Phys. B **130**, 505 (1977).
- [16] R. Teh, B.L. Ng and K.M. Wong, Ann. Phys. (N. Y.), **362**, 170 (2016).
- [17] D. Zhu, K.M. Wong and G.Q. Wong, sent for publication.
- [18] P.A. Zyla et al. (Particle Data Group), Prog. Theor. Exp. Phys. **2020**, 083C01 (2020).